iScience

CellPress
OPEN ACCESS

Article

YAP condensates are highly organized hubs

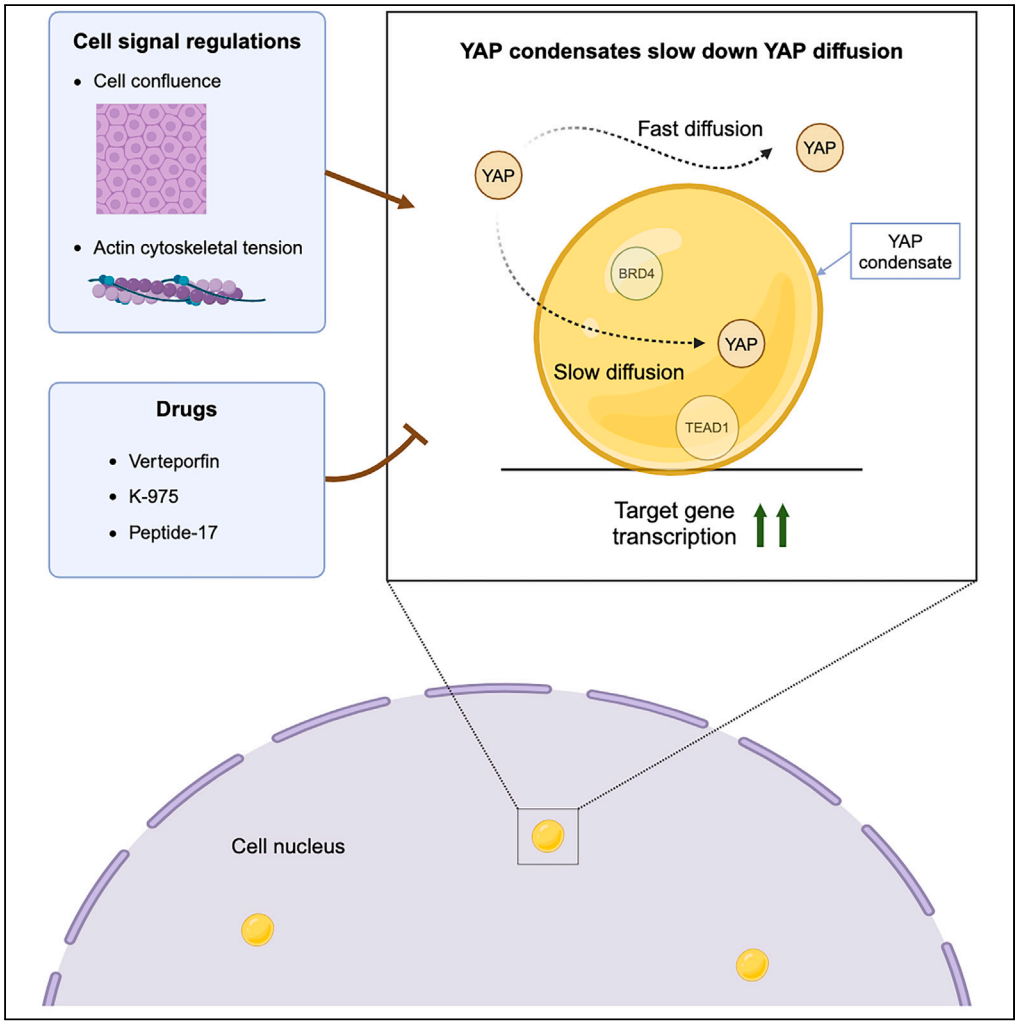

Siyuan Hao, Ye Jin Lee, Nadav Benhamou Goldfajn, ..., Zhe Liu, Shahar Sukenik, Danfeng Cai

danfeng.cai@jhu.edu

Highlights

YAP condensates are responsive to cell confluence signals and cytoskeletal tension

TEAD1 stabilizes YAP condensates, which further recruits BRD4 for transcription

Drugs are effective at rapidly disrupting YAP condensates

YAP condensates slow down YAP diffusion within condensate boundaries

Hao et al., iScience 27, 109927
June 21, 2024
https://doi.org/10.1016/j.isci.2024.109927

iScience

CellPress
OPEN ACCESS

Article

YAP condensates are highly organized hubs

Siyuan Hao,[1] Ye Jin Lee,[1] Nadav Benhamou Goldfajn,[1,2] Eduardo Flores,[3] Jindayi Liang,[1] Hannah Fuehrer,[1] Justin Demmerle,[1] Jennifer Lippincott-Schwartz,[6] Zhe Liu,[6] Shahar Sukenik,[3] and Danfeng Cai[1,4,5,6,7,*]

SUMMARY

YAP/TEAD signaling is essential for organismal development, cell proliferation, and cancer progression. As a transcriptional coactivator, how YAP activates its downstream target genes is incompletely understood. YAP forms biomolecular condensates in response to hyperosmotic stress, concentrating transcription-related factors to activate downstream target genes. However, whether YAP forms condensates under other signals, how YAP condensates organize and function, and how YAP condensates activate transcription in general are unknown. Here, we report that endogenous YAP forms sub-micron scale condensates in response to Hippo pathway regulation and actin cytoskeletal tension. YAP condensates are stabilized by the transcription factor TEAD1, and recruit BRD4, a coactivator that is enriched at active enhancers. Using single-particle tracking, we found that YAP condensates slowed YAP diffusion within condensate boundaries, a possible mechanism for promoting YAP target search. These results reveal that YAP condensate formation is a highly regulated process that is critical for YAP/TEAD target gene expression.

INTRODUCTION

Yes-associated protein (YAP) is a transcriptional coactivator that plays important roles in development and diseases such as cancer. Together with TEA domain (TEAD) transcription factors, they transcribe target genes important for cell proliferation and survival.[1] YAP/TEAD activities are tightly controlled by the Hippo signaling pathway, a kinase cascade involving MST1/2 and LATS1/2 that ultimately phosphorylates and restricts YAP or its paralog PDZ-binding motif (TAZ) in the cytoplasm, thus limiting their transcriptional activities.[2,3] YAP is also sensitive to cell mechanical regulations. Mechanical forces[4–6] and hyperosmotic stress[7] both influence the nuclear translocation and transcriptional activity of YAP, but how YAP and TEAD mediate target gene expression is still unresolved. Recent data shows that YAP and TEAD interact with other transcriptional activators such as Mediator and Bromodomain Containing 4 (BRD4), all of which bind to super-enhancer regions.[8,9] However, the molecular organization of YAP/TEAD transcription complexes is unknown.

New studies from our lab and those of others confirm that YAP and TAZ both form liquid-like biomolecular condensates during active transcription.[10–13] Biomolecular condensates are membrane-less compartments inside cells formed by weak, multivalent interactions among proteins or nucleic acids. Many biomolecular condensates enrich components within the same signaling pathway and they can accelerate biochemical reactions.[14–16] We have found that in response to hyperosmotic stress, YAP forms condensates that enrich TEAD1, reorganize accessible chromatin domains, and upregulate transcription.[10] Whether YAP condensate formation is a general phenomenon accompanying high YAP activity, how YAP condensates are organized, and the biophysical properties of YAP condensates remain unknown. A detailed understanding of these questions will provide a mechanistic understanding of how YAP condensates promote transcription.

Here we focus on endogenous YAP condensates under other physiologically relevant signals that could affect YAP activity. We find that YAP condensate formation is regulated by both Hippo signaling and actin cytoskeletal tension. YAP condensates organize in a hierarchical fashion: TEAD1 promotes YAP condensation, which recruits the transcriptional activator BRD4 for gene activation. Using single-particle tracking (SPT) to monitor intracellular YAP dynamics, we investigated the biophysical properties of YAP condensates and find them to be a viscous environment that can slow down YAP diffusion. Our findings reveal important insights into how YAP condensates can be organized and regulated to mediate gene expression.

[1]Department of Biochemistry and Molecular Biology, Johns Hopkins Bloomberg School of Public Health, Baltimore, MD 21205, USA
[2]Department of Biophysics, Johns Hopkins University, 3400 N. Charles St., Baltimore, MD 21218, USA
[3]Department of Chemistry and Chemical Biology, University of California, Merced, Merced, CA 95343, USA
[4]Department of Biophysics and Biophysical Chemistry, Johns Hopkins School of Medicine, Baltimore, MD 21205, USA
[5]Department of Oncology, Johns Hopkins School of Medicine, Baltimore, MD 21205, USA
[6]Janelia Research Campus, Howard Hughes Medical Institute, Ashburn, VA 20147, USA
[7]Lead contact
*Correspondence: danfeng.cai@jhu.edu
https://doi.org/10.1016/j.isci.2024.109927

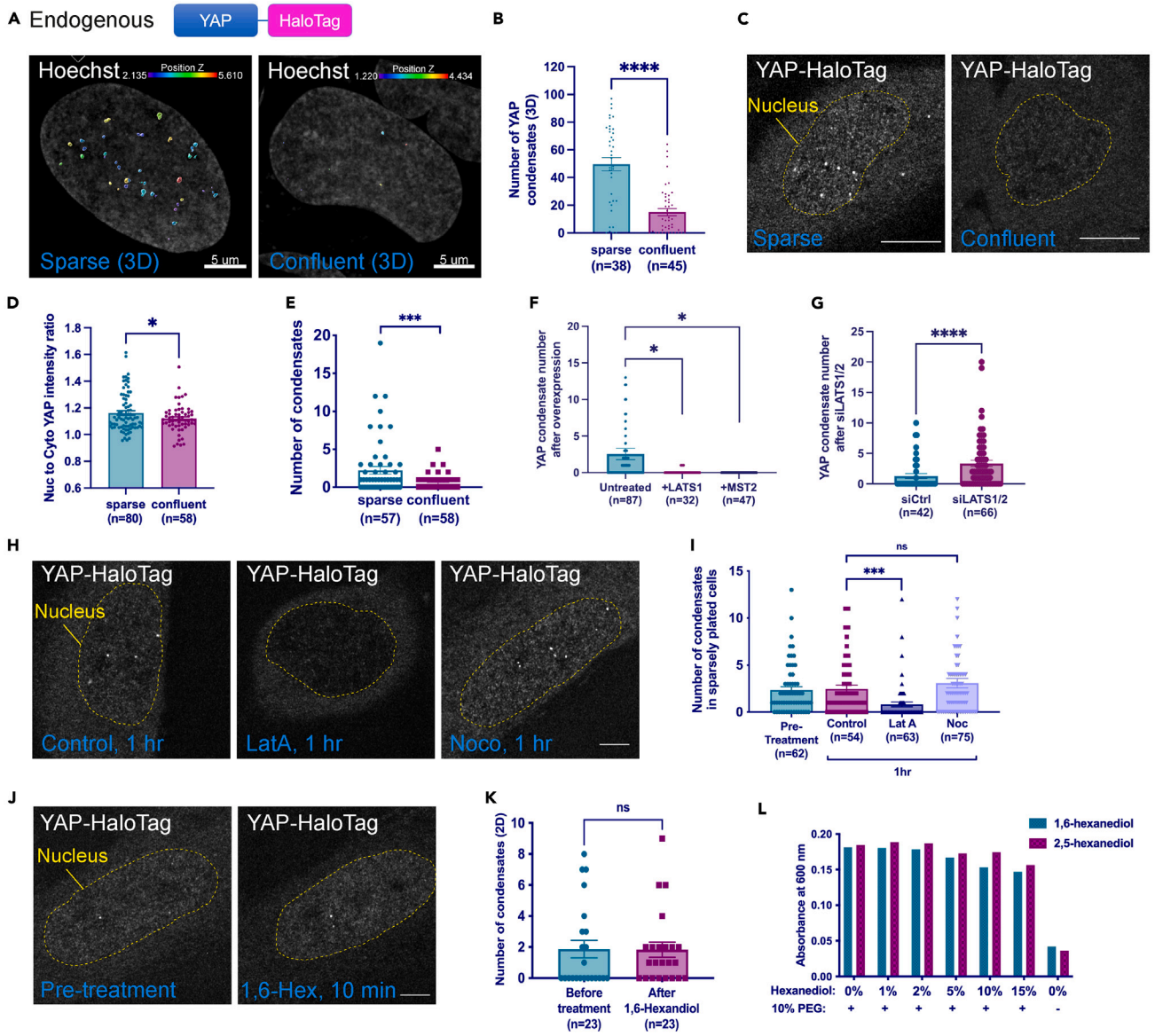

Figure 1. YAP condensates are regulated by Hippo pathway and mechanical tension

(A) Representative 3D Airyscan images of sparse and confluent U-2 OS cells containing YAP-HaloTag (graphically depicted above the images) and labeled with JF549 Halo dye,[17] processed with maximum intensity projection with Imaris software (Bitplane). YAP condensates are identified by surface detection module (Imaris) and color-coded statistically by their z-positions.

(B) Number of YAP condensates in sparse and confluently plated U-2 OS YAP-HaloTag cells in the whole nucleus in 3D. ****: statistically significant difference in the YAP condensate number between sparse and confluent samples ($p < 0.0001$, unpaired t test). The center of the data is the mean, and the error bars show the s.e.m.

(C) Representative 2D Airyscan images of U-2 OS cells containing YAP-HaloTag, plated sparsely and confluently and labeled with JF549 Halo dye. Scale bars: 10 μm.

(D) Nuclear to cytoplasmic YAP intensity ratio in sparsely versus confluently plated U-2 OS YAP-HaloTag cells calculated from 2D images. *: statistically significant difference ($p < 0.05$, unpaired t test). The center of the data is the mean and the error bars show the s.e.m.

(E) Number of YAP condensates in sparse and confluently plated U-2 OS YAP-HaloTag cells in 2D. ***: statistically significant difference in the YAP condensate number between sparse and confluent samples ($p < 0.001$, unpaired t test). The center of the data is the mean, and the error bars show the s.e.m.

(F–G) Number of YAP condensates in Hippo pathway overexpressing, sparse U-2 OS YAP-HaloTag cells (F) and control and LATS1/2 siRNA knockdown, confluent U-2 OS YAP-HaloTag cells (G) imaged in 2D. *: statistically significant difference in the YAP condensate number between control, LATS1-GFP, and MST2-GFP overexpressed samples ($p < 0.05$, one-way ANOVA test). ****: statistically significant difference in the YAP condensate number between control siRNA and LATS1/2 siRNA-treated samples ($p < 0.0001$, unpaired t test). The center of the data is the mean and the error bars show the s.e.m.

Figure 1. *Continued*

(H) Representative 2D Airyscan images of U-2 OS YAP-HaloTag cells treated with DMSO (control), Latrunculin A (LatA) (0.1 μg/ml), or Nocodazole (Noco) (30 μM), respectively, for 1 h, and labeled with JF549 Halo dye. Scale bar: 5 μm.

(I) Number of YAP condensates in sparsely plated U-2 OS YAP-HaloTag cells in 2D, at pre-treatment and 1 h after DMSO control, Latrunculin A (0.1 μg/ml) or Nocodazole (30 μM) treatments. ***: statistically significant difference in the YAP condensate number between DMSO and Latrunculin A-treated samples ($p < 0.001$, unpaired t test). NS: non-significant difference between DMSO and Nocodazole-treated samples (unpaired t test). The center of the data is the mean and the error bars show the s.e.m.

(J) Representative 2D Airyscan images of a U-2 OS YAP-HaloTag cell pre-treatment and after 10 min of 1% 1,6-hexandiol treatment, labeled with JF549 Halo dye. Scale bar: 5 μm.

(K) Number of YAP condensates in U-2 OS YAP-HaloTag cells in 2D pre-treatment and after 10 min of 1% 1,6-hexandiol treatment. ns: non-significant difference between samples (paired t test). The center of the data is the mean and the error bars show the s.e.m.

(L) Absorbance values (at 600 nm wavelength) of purified YAP full length protein in solution (with and without 10% PEG), treated with the indicated percentage of 1,6-hexandiol or 2,5-hexandiol.

RESULTS

Yes-associated protein condensates are regulated by the Hippo pathway and mechanical tension

To test how YAP condensation can be regulated by other physiologically relevant signals, we utilized a U-2 OS cell line where the endogenous YAP protein is labeled with a HaloTag (U-2 OS YAP-HaloTag, Figure 1A), in which YAP-HaloTag forms liquid-like nuclear condensates at endogenous YAP expression levels,[10] colocalizing with YAP target gene *MYC*[18,19] but not non-target *ACTB* as shown by intron RNA FISH against *MYC* or *ACTB* nascent transcripts (Figures S1A–S1C). Tagging YAP c-terminally with HaloTag did not influence the normal activity of YAP, since: 1) YAP-HaloTag expression level is similar to WT YAP in the parental cell line (Figures S1D and S1F) 2) YAP-HaloTag had a similar ability to bind to the transcription factor TEAD1 as wildtype YAP in different cell confluence conditions (Figures S1D and S1E); 3) YAP-HaloTag nuclear localization responded to cell confluence, showing higher nuclear localization in sparse cells than in confluent cells (Figures 1C, 1D, S1D, and S1F); 4) U-2 OS YAP-HaloTag cell line had similar level of YAP/TEAD target gene expression as the parental U-2 OS cell line, in both sparse and confluenct cell conditions (Figures S1G and S1H); and 5) YAP condensates in both parental U-2 OS and YAP-HaloTag cell lines are not protein aggregates since they are negative for an amyloid marker AmyTracker680 (Figures S1I–S1O). Like YAP nuclear localization, YAP condensate formation is also regulated by cell confluence. In sparsely plated cells, around 50 YAP condensates form inside the cell nucleus (or 2–3 per 2D plane), but when cell density is high, nuclear YAP condensate number decreases to around 15 per nucleus (or 0–1 per 2D plane) (Figures 1A–1C and 1E). These results indicate that cell density regulates YAP condensate formation. For ease of quantification, we will be showing images and data quantifying nuclear YAP condensates on the 2D plane. We predicted that cell confluence regulates YAP condensation through the Hippo pathway, because the Hippo pathway is known to respond to cell confluence and YAP is regulated by the Hippo pathway.[2,3] We modulated Hippo pathway activity in U-2 OS YAP-HaloTag cells by overexpressing the Hippo pathway components MST2 or LATS1,[20] or by knocking down LATS1 and LATS2 with siRNAs. Hippo pathway activation normally leads to decreases in the expression of YAP target genes. Attesting to the effectiveness of these approaches, YAP nuclear intensity decreased after overexpressing either LATS1 or MST2 (Figure S1P), and YAP target gene *CYR61 (*i.e., *CCN1)* increased expression after LATS1/2 knockdown (Figure S1R). Consistent with our hypothesis, overexpressing either of the Hippo pathway components MST2 or LATS1 dramatically reduced the number of YAP condensates (Figure 1F), while knocking down LATS1 and LATS2 with siRNA significantly increased the number of YAP condensates, even when cells were plated at high density (Figure 1G). Interestingly, the increase in the YAP condensate number after LATS1/2 siRNA was not coupled to an increase in YAP nuclear intensity (Figure S1Q). These results all indicate that cell confluence, likely signaled through the Hippo pathway, can regulate YAP condensate formation.

Extracellular mechanical forces are known to regulate the nuclear localization of YAP and YAP/TEAD transcriptional activity.[4–6] These mechanical forces are sensed and transduced by the cytoskeleton.[5] To determine if mechanical signals can affect YAP activity by regulating YAP condensate formation, we disrupted the actin cytoskeleton with latrunculin A, a drug that blocks actin polymerization.[21,22] We found that YAP condensates disappeared within 1 h of actin disruption (Figures 1H and 1I), accompanied by a decrease in YAP nuclear intensity (Figure S1S) and decrease in the expression of YAP target genes *CTGF (*i.e., *CCN2)* and *CYR61* (Figure S1T). Cytoskeletal regulation of YAP condensation is specific to actin, since disrupting the microtubule network with the microtubule-specific drug nocodazole[23] had no effect on YAP condensate formation (Figures 1H and 1I) and didn't decrease YAP nuclear intensity or target gene expression (Figures 1H, S1S, and S1T). This indicates that YAP condensation is sensitive to mechanical forces mediated specifically by the actin cytoskeleton. Notably unlike many other biomolecular condensates,[24–27] YAP condensates could not be dissolved by the aliphatic alcohol 1,6-hexanediol *in cell* (Figures 1J and 1K), despite the condensation of the surrounding chromatin that was a hallmark of 1,6-hexandiol treatment[28,29] (Figure S1U). YAP condensates formed *in vitro* were also not disrupted by either 1,6- or 2,5-hexanediol (Figure 1L).[24] These results suggest that YAP condensates have distinct biophysical properties from the condensates formed by proteins such as Fused in sarcoma (FUS) and TAR DNA binding protein 43 (TDP-43),[24] and are specifically regulated by both the Hippo pathway and the actin cytoskeleton.

TEA domain 1 transcription factor stabilizes Yes-associated protein condensate

YAP can bind to a number of transcription factors (TFs) such as TEAD, p73, and Runx,[30–32] but only YAP-TEAD binding promotes growth and survival-related downstream gene transcription.[1,31] Both the osmotically and mechanically induced YAP condensates contain and concentrate TEAD1 protein (Figures 2A–2C),[10] but the function of TEAD1 in YAP condensate formation remains unknown. To test the roles of

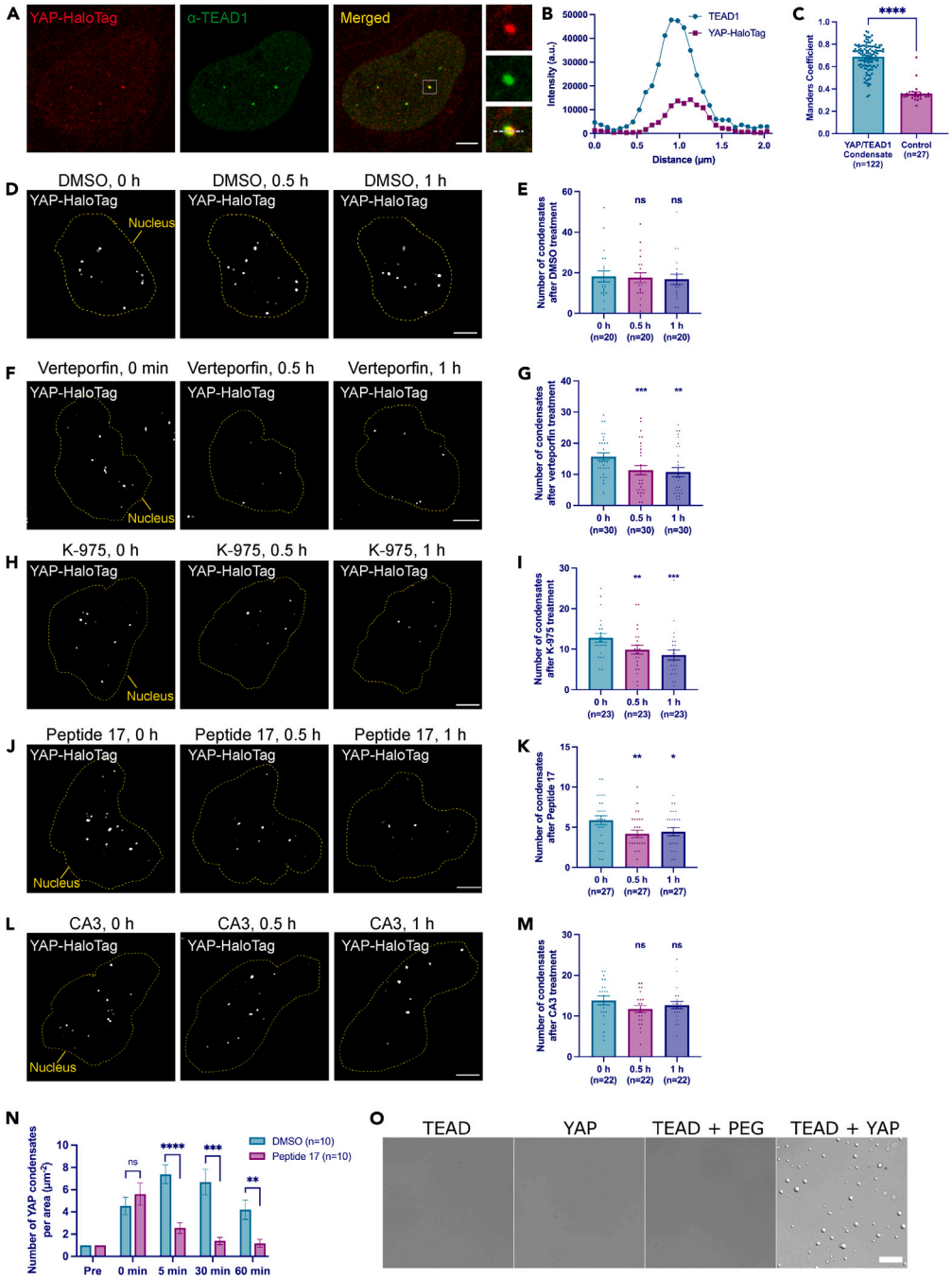

Figure 2. TEAD1 transcription factor stabilizes YAP condensate

(A) Representative 2D confocal immunofluorescence image of a U-2 OS YAP-HaloTag cell plated sparsely, showing both YAP and TEAD1 foci. Magnification of the inset in the merged image. Scale bar: 5 μm.

(B) Line scan of the dotted line in the magnified image from (A) showing the overlap of YAP and TEAD1 condensates.

(C) Quantification of colocalization between YAP condensates with TEAD1 foci using Mander's coefficient. ****: statistically significant difference between YAP condensate/TEAD1 foci colocalization and random nuclear region/TEAD1 foci colocalization ($p < 0.0001$, unpaired t test). The center of the data is the mean and the error bars show the s.e.m.

(D–M). Live-cell 2D Airyscan images of sparsely plated U-2 OS YAP-HaloTag cells treated with DMSO (D), 50 nM verteporfin (F), 500 nM K-975 (H), 500 nM Peptide 17 (J), and 500 nM CA3 (L) at the indicated time after treatment. Scale bars: 5 μm. Quantification of the YAP condensate numbers in 2D in (E, G, I, K, M) after treatment with each drug at the indicated time. *, **, ***: statistically significant differences in the YAP condensate number between pre-treatment and drug-treated samples (*: $p < 0.05$, **: $p < 0.01$, ***: $p < 0.001$, paired t test). ns: non-significant difference between samples (paired t test). The center of the

Figure 2. *Continued*

data is the mean and the error bars show the s.e.m. The average number of condensates during pre-treatment is higher than calculated in Figure 1 since only cells containing at least one YAP condensate were analyzed for drug treatments.

(N) Normalized number of YAP condensates in 2D in sorbitol-treated, sparsely plated U-2 OS YAP-HaloTag cells per nuclear area, with additional DMSO or Peptide 17 treatments over 1 h. **, ***, ****: statistically significant difference in the YAP condensate number between DMSO and Peptide 17-treated samples at indicated time points (**: $p < 0.01$, ***: $p < 0.001$, ****: $p < 0.0001$. Unpaired t test). ns: non-significant difference between samples at 0 min (unpaired t test). The center of the data is the mean and the error bars show the s.e.m.

(O) Differential Interference Contrast (DIC) images of purified TEAD1 (20 μM) and YAP (15 μM) proteins alone, TEAD1 (15 μM) with crowding agent 20% (w/w) PEG 2k, and TEAD1 (15 μM) and YAP (15 μM) mixed together, showing that mixing of YAP and TEAD1 promotes the phase separation of both proteins. Scale bar is 20 μm.

TEAD1 in YAP condensation, we treated U-2 OS YAP-HaloTag cells with drugs that are known to disrupt YAP-TEAD interactions. Specifically, verteporfin is a benzoporphyrin derivative that binds to the WW domain of YAP altering its conformation and interactions with TEAD;[33–35] K-975 is a chemical that binds to the YAP-binding pocket of TEAD, inhibiting its binding with YAP;[36] and Peptide 17 is a slightly mutated fragment of YAP that binds to TEAD with high affinity and competes with endogenous YAP binding.[37–39] We then quantified the number of YAP condensates before and after drug treatments with live-cell imaging. Within 30 min of treatment with K-975 or Peptide 17, the Pearson's R value of colocalization between the YAP and TEAD1 signals decreased (Figures S2A and S2B), indicating that K-975 and Peptide 17 are effective in disrupting YAP/TEAD1 interactions. We discovered that compared with DMSO-treated cells in which the YAP condensate number, intensity, and area didn't change (Figures 2D, 2E, S2C, and S2D), the number of YAP condensates decreased within 30 min of verteporfin (Figures 2F and 2G), K-975 (Figures 2H and 2I), and Peptide 17 (Figures 2J and 2K) treatments, demonstrating that the YAP-TEAD1 interaction is necessary for YAP condensate formation. Interestingly, these drugs decreased the YAP condensate number without affecting YAP nuclear localization (Figures S2E-S2H). However, YAP transcription activity decreased (Figures S2I and S2J) after K-975 treatment, indicating that YAP condensation is mainly responsible for the transcriptional activities of YAP. CA3 is a novel YAP inhibitor that decreases YAP expression through an unknown mechanism.[40] Within 1 h of CA3 treatment, the number of YAP condensates remained the same (Figures 2L and 2M), indicating that directly modulating YAP/TEAD1 interaction is more effective in interrupting YAP condensate formation. To rule out the potential off-target effects of the drug treatments, and to verify the involvement of TEAD1 in YAP condensate formation, we knocked down TEAD1 expression in U-2 OS YAP-HaloTag cells using siRNA (Figure S2K) and found that the number of YAP condensates significantly decreased (Figure S2L) concurrent with YAP nuclear intensity decrease (Figure S2M). These results all indicate that TEAD1 positively regulates YAP condensation. TEAD1 could regulate YAP condensation either by promoting YAP condensate formation, or by decreasing YAP condensate dissolution. To distinguish between these possibilities, we pre-treated cells with Peptide 17 for 1 h and then induced YAP condensate formation with sorbitol before monitoring the dynamics of YAP condensate formation. Consistent with previous reports,[10] sorbitol treatment in drug-free conditions rapidly induced the formation of YAP condensates, which then gradually dissolved around 1 h after sorbitol treatment (Figures 2N and S2N). Interestingly, pretreatment of cells with Peptide 17 did not change the rate of YAP condensate formation upon hyperosmotic stress, but significantly accelerated YAP condensate dissolution (Figures 2N and S2N), indicating that the YAP-TEAD1 interaction is mainly responsible for stabilizing YAP condensates after their formation. Consistent with these in-cell results, we found that while purified YAP protein can form phase separated droplets *in vitro* at high concentrations[10] (Figure S2O), the addition of purified TEAD1 protein caused YAP to phase separate at much lower concentrations (Figure 2O), and in a TEAD1 concentration-dependent fashion (Figure S2O). Together, these results indicate that TEAD1 promotes YAP condensate stabilization after its formation, and facilitates YAP condensate formation at a lower concentration of YAP.

Yes-associated protein condensates recruit mediator and bromodomain containing 4 to mediate transcription

The binding of YAP/TAZ to TFs is often enriched at super enhancers (SEs)[8,9] which are enhancers that activate high levels of cell type-specific gene expression.[41,42] We previously proposed that YAP condensates localize at SEs because both YAP condensates and SEs are enriched at clusters of accessible chromatin regions (ACDs).[10] To determine if YAP condensates are present at areas of active transcription, we asked whether YAP condensates also contain BRD4, a transcriptional coactivator that binds to transcriptionally active, acetylated SE regions.[43,44] Previously, it was shown that TAZ condensates formed after the overexpression of TAZ can enrich BRD4.[13] However, it is unknown whether condensates of YAP (a paralog of TAZ that is known to have non-redundant functions[45,46]) formed endogenously can also enrich BRD4. Consistent with previous observations,[26] we found that endogenous BRD4 forms distinct condensates inside the nucleus (Figure 3A). Importantly, many of these BRD4 condensates are also YAP condensates, since in sparsely plated cells with high YAP activity almost every YAP condensate overlapped with a BRD4 condensate (Figures 3A and 3B). To test whether BRD4 is necessary for YAP condensate formation, or if it is only recruited to YAP condensates after their formation, we treated cells with JQ-1, a drug specifically targeting the BET family of bromodomain proteins that includes BRD4.[47] We found that while mean YAP nuclear intensity and the number of YAP condensates remained the same after 1 h of JQ-1 treatment (Figures 3C, 3E, and 3F), BRD4 formed significantly fewer condensates inside the nucleus and was no longer concentrated at YAP condensates (Figures 3C, 3D, and 3H). Instead, BRD4 became diffusely localized inside the nucleus and had a higher overall intensity throughout the nucleoplasm (Figures 3C and 3G). However, at individual YAP condensates, BRD4 intensity significantly decreased (Figures S3A–S3C). To determine the change in BRD4 accumulation at YAP condensates, we averaged together images of many YAP condensates in both DMSO and JQ-1 treated cells (Figure 3I), and measured the average intensity of both YAP and BRD4 in the averaged images. We found that while YAP condensate intensity remained

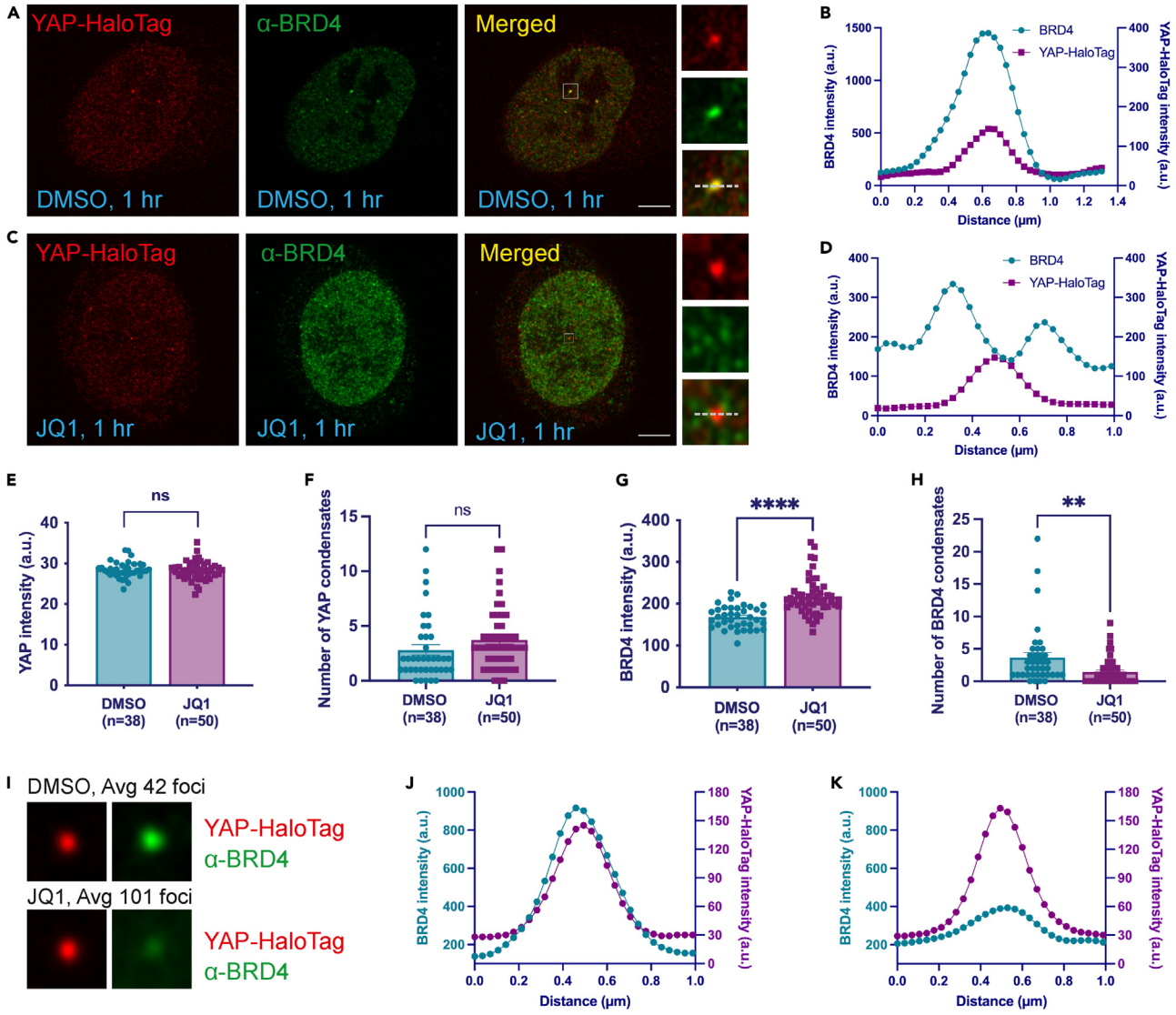

Figure 3. YAP condensates recruit BRD4 to mediate transcription

(A and C) Representative 2D confocal immunofluorescence images of sparsely plated U-2 OS YAP-HaloTag cells showing YAP and BRD4 staining after 1 h of DMSO (A) or 1 μM JQ-1 (C) treatment. The insets are the magnification of the boxes in the merged images. The boxes are centered around YAP condensates. Scale bar: 5 μm.

(B and D) Line scans of the dotted line in the magnified images in (A, C) showing overlap (B) and lack of overlap (D) of YAP and BRD4 channels.

(E and G) Quantifications of mean nuclear YAP intensity (E) and mean nuclear BRD4 intensity (G) after 1 h DMSO or JQ-1 (1 μM) treatments in sparsely plated U-2 OS YAP-HaloTag cells. **: statistically significant difference in BRD4 intensity between DMSO and JQ-1-treated samples (****: $p < 0.0001$, unpaired t test). ns: non-significant difference in YAP intensity between samples (unpaired t test). The center of the data is the mean and the error bars show the s.e.m.

(F and H) Quantifications of the number of YAP condensates (F) and BRD4 condensates (H) in 2D after DMSO and JQ-1 (1 μM) treatments in sparsely plated U-2 OS YAP-HaloTag cells. ****: statistically significant difference in BRD4 condensate number between DMSO and JQ-1-treated samples (**: $p < 0.01$, unpaired t test). ns: non-significant difference in the YAP condensate number between samples (unpaired t test). The center of the data is the mean and the error bars show the s.e.m.

(I) Averaged images centered on YAP condensates in 2D in sparsely plated U-2 OS YAP-HaloTag cells, showing a decreased average BRD4 intensity after 1 h of JQ-1 (1 μM) treatment.

(J and K) Line plots of YAP-HaloTag and BRD4 average intensity from (I) after 1 h of DMSO treatment (J) or JQ-1 (1 μM) treatment (K). Cyan line: BRD4 intensity; magenta line: YAP-HaloTag intensity visualized with JF549 Halo Dye.

unchanged, BRD4 intensity at YAP condensates decreased by more than 50% after JQ-1 treatment (Figures 3I–3K). Accordingly, we found that the expression of many genes co-regulated by YAP/TAZ and BRD4[9] decreased after JQ-1 treatment (Figures S3D–S3N) while the level of internal control GAPDH didn't change (Figure S3O). These results suggest that BRD4 is not necessary for YAP condensate

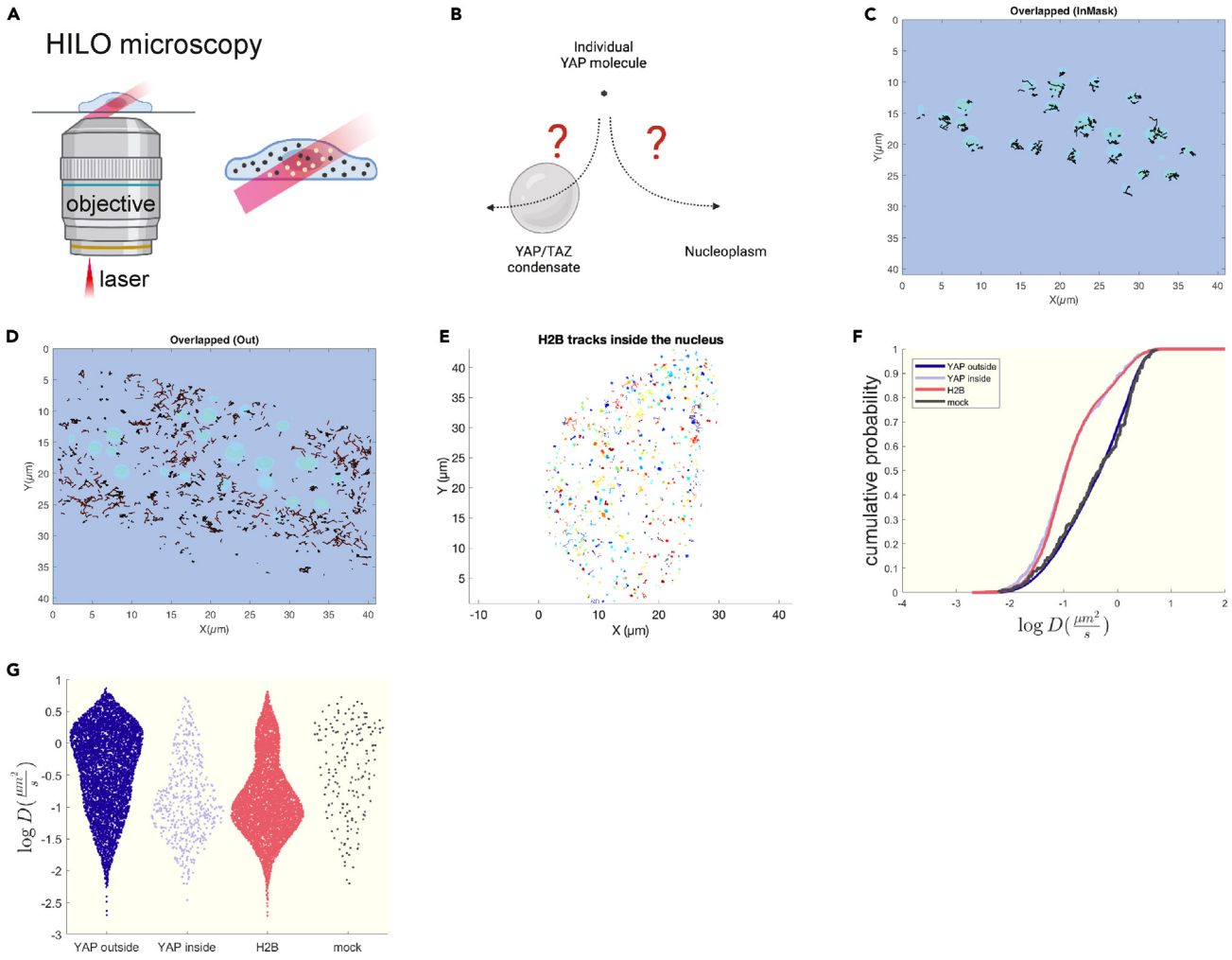

Figure 4. Phase separation slows down YAP diffusion

(A) Illustration of HILO microscopy principle: an inclined light sheet comes out of the objective and illuminates a thin section in the cell. Only molecules in that plane are illuminated.

(B) Illustration showing strategies to track single YAP molecules inside and outside YAP/TAZ condensates.

(C and D) Individual tracks of YAP-HaloTag molecules in sparsely plated U-2 OS YAP-HaloTag cells from an SPT experiment showing those trajectories overlapping with YAP/TAZ condensates (C) and those not overlapping with YAP/TAZ condensates (D). YAP/TAZ condensates were pseudo-colored in light blue.

(E) Individual tracks of H2B-HaloTag molecules from an SPT experiment showing mostly stationary H2B molecules.

(F) Cumulative plots of diffusion coefficients of H2B molecules (red), YAP molecules inside EGFP-TAZ condensates (purple) and mock compartments (gray), and YAP molecules outside condensates (blue).

(G) Comparison of all diffusion coefficients of H2B molecules, YAP molecules inside condensates and mock compartments, and YAP molecules outside condensates.

formation, but is instead recruited to YAP condensates, likely by binding to acetylated transcriptional regulators, and thus leads to elevated YAP target gene expression. These results, coupled with previous finding that YAP bound to SEs could enrich BRD4,[9] indicated that YAP condensates indeed localize at SEs mediating active transcription.

Phase separation slows down Yes-associated protein diffusion

While the mechanisms of YAP localization to the nucleus have been widely studied, how YAP mediates transcription once it is inside the nucleus is not completely understood. Phase separation of transcription-related factors may create a distinct environment for molecules inside the condensates, facilitate the target search of TFs for their DNA binding sequences, and promote gene transcription.[42,48] To understand how the internal environment of YAP condensate influences YAP activity, we used SPT to follow the trajectories of individual YAP molecules as they traveled, both within the nucleoplasm and inside of YAP condensates. To achieve high signal-to-background sensitivity, we used highly inclined and laminated optical sheet (HILO) microscopy[49] on a custom-built Nikon Ti-E microscope to visualize trajectories of individual YAP

molecules (Figures 4A and S4A, Video S1). We found that inside a single nucleus, YAP molecules can be fast-diffusing (Video S2) and slow-diffusing (Video S3). To understand how condensates influence YAP diffusion (Figure 4B), we used EGFP-TAZ condensates as references (Figure S4B), since endogenous YAP condensates are too small to reliably segment the single molecule trajectories, and TAZ is known to form phase-separated bodies that are co-occupant with YAP condensates.[10,13] We observed that YAP molecules within the boundaries of YAP/TAZ condensates diffuse much more slowly than YAP molecules outside of YAP/TAZ condensates (Figures 4C, 4D, 4F, and 4G, Video S4). As a control, we computationally randomly generated compartments inside the nucleus (Figure S4C) and observed that YAP diffusion didn't slow down in these mock compartments (Figures 4F and 4G). We conclude that YAP diffusion slows down within the phase-separated YAP/TAZ condensates, likely due to the many weak multi-valent interactions between YAP, TAZ, and TEAD1. We compared these results to SPT data from Halo-tagged histone H2B, an integral component of nucleosomes with a low diffusion coefficient ($\sim$0.01 $\mu m^2/s$, Figure 4E). The slowly diffusing YAP molecules inside the YAP/TAZ condensates have diffusion coefficients close to those of H2B, but slower than those of YAP molecules outside of condensates (Figures 4F and 4G), indicating that rapidly diffusing YAP proteins are slowed down by multivalent protein: protein or protein: DNA interactions locally within condensates. This change in diffusion rate could in theory promote YAP-mediated transcription by facilitating the target search of YAP-interacting TFs.

DISCUSSION

Here we report that YAP condensates can be regulated by physiologically relevant signals such as Hippo pathway signaling and cell mechano-regulation. This finding challenges the current hypothesis that YAP condensates are absent in homeostatic conditions and can only be induced by external stimuli such as hyperosmotic stress or interferon-γ.[11,12,50] These findings are made possible by investigating endogenous YAP dynamics using super resolution imaging in living cells, as endogenous YAP condensates are small (less than a micron in diameter) and can be disrupted by cell fixation.[51] Our finding that YAP forms biomolecular condensates during homeostasis is important for understanding YAP-mediated transcription in general, and provides a framework for understanding how YAP, as a master transcriptional regulator important in development and cancer, concentrates transcription-related factors to mediate downstream gene expression.

One interesting discovery is that YAP forms around 50 condensates in sparsely plated cells, which is at odds with previous findings showing that YAP can bind to hundreds of enhancer sites.[8] We think it can be explained by one YAP condensate regulating multiple genes, supported by our previous finding that individual YAP condensate localizes to clustered accessible chromatin domains.[10] It is not uncommon for transcription-related factors to co-regulate multiple genes. For example, the number of foci formed by LDB1 (LIM Domain Binding 1, a co-activator that controls motor neuron development) is orders of magnitude fewer than LDB1 peaks on the genome as identified by ChIP-seq (unpublished and[52]), indicating that one LDB1 foci can regulate multiple genes. With that said, to show definitively that YAP condensate regulates multiple genes, further studies using approaches to detect multiple YAP target genes such as MERFISH[53] will be needed. On the other hand, YAP still forms around 15 condensates in confluent cells when they are supposedly inactive. While previous studies have shown that YAP is still able to bind to the chromatin under inactive conditions,[54,55] we speculate that YAP condensates in YAP-inactive condition may bookmark the important genes and prepare them for transcriptional activation once cells are placed sparsely and YAP becomes active. This is similar to the scenario when the TF Sox2 (SRY-box 2) binds to the mitotic chromosome in mouse embryonic stem cells and prepare the cells for transcription once mitosis ends.[56] Alternatively, since YAP/TEAD1 condensates can form *in vitro* in the absence of DNA (Figure S2O), it is probable that YAP condensates in cell can be involved in functions other than transcription regulation. Future research will be done to test these interesting hypotheses.

TFs and coactivators need to find and bind to hundreds or thousands of specific genomic sites out of tens or hundreds of thousands of possible binding sites, and recruit specific proteins to mediate transcription. How they reliably accomplish this important task has been an outstanding question in the field. Recently, with the advent of new SPT technology to track individual TF and coactivators molecules, it was discovered that the distributions of TFs like Sox2 and the glucocorticoid receptor within the nucleus are not random; instead, they form clusters to slow down TF and cofactor diffusion, thereby aiding in the search for TF binding sites.[57,58] However, the nature of those TF and coactivator clusters are relatively uncharacterized, and they have been proposed to be phase-separated condensates. There are a couple of conceivable benefits of TFs forming phase-separated compartments: firstly, thanks to the surface tension from a phase-separated compartment, molecules are more likely to stay inside the compartment than leaving it. It provides benefits such as helping transcription-related factors find their cognate binding sites. Secondly, due to the absence of membranes, molecules can still diffuse through the boundary of these phase-separated compartments. This semi-permeability is the main benefit of creating phase-separated compartments. Indeed, using SPT, we found that YAP/TAZ condensates slow down the diffusion of YAP inside the condensates. This finding provides important evidence that biomolecular condensates are critical for TF and coactivator target search. Boundary effects are especially important in small liquid-like droplets because of their higher surface area to volume ratios. In our current study, we used larger YAP/TAZ condensates as they are easier than small endogenous YAP condensates to segment the tracks, while sharing similar biophysical properties as endogenous YAP condensates.[10] In fact, previous attempts to measure molecule diffusion across condensates from other labs have all used larger condensates resulted from protein overexpression.[59,60] In the future, we hope to develop better methods to segment tracks across smaller condensates, which will reveal how condensates of different sizes affect protein function differently inside the nucleus.

Since condensates are intimately linked to various forms of diseases including neurodegeneration[61,62] and cancer,[63–65] condensate-targeting therapies have garnered attention in recent years. Early attempts to modulate condensates involved using chemicals such as 1,6-hexandiol or targeting nuclear import receptors.[66] These methods, while often effective in disrupting condensates of interest, suffered from high

toxicity and a lack of specificity. Recently, new methods have emerged to target disease-related condensates, including modulating condensate composition, targeting the molecular interactions among condensate components, and modulating condensate regulatory processes.[63,67] Despite these progresses, and the potential involvement of YAP condensates in cancer, there is currently no effective way to modulate YAP condensates. This study is the first to report pharmacological compounds that can specifically disrupt YAP condensates. We report that three drugs, verteporfin, Peptide 17, and K-975 are effective in rapidly decreasing the number of YAP condensates. As known disruptors of YAP/TEAD interactions, the use of verteporfin, Peptide 17 and K-975 also reveal the key role of the TF TEAD1 in stabilizing YAP condensates. Our results point to a fruitful avenue of repurposing existing YAP and Hippo pathway-targeting drugs to modulate YAP condensates. In the future, we will test a comprehensive panel of drugs to find more small molecules or peptides that can regulate YAP condensate formation. However, using these drugs for patient treatments is still a distant hope. To achieve the local delivery of these compounds to diseased tissues, we need to find chemical vehicles that can envelop and protect these drugs, and target them to specific sites (such as tumors) for potential therapeutic outcomes.

Limitations of the study

We observe an immediate impact of multiple drugs on the number of YAP condensates shortly after treatment. However, the long-term effects of these drugs on YAP condensates have not been assessed, and their efficacy within a tissue environment remains unknown. During SPT, we utilized larger EGFP-TAZ condensates as substitutes for YAP condensates, as endogenous YAP condensates are too small for track segmentation. Future research should aim to explore the influence of smaller YAP condensates on YAP diffusion.

STAR★METHODS

Detailed methods are provided in the online version of this paper and include the following:

- KEY RESOURCES TABLE
- RESOURCE AVAILABILITY
  - Lead contact
  - Materials availability
  - Data and code availability
- EXPERIMENTAL MODEL AND STUDY PARTICIPANT DETAILS
  - Cell lines
- METHOD DETAILS
  - Transfection and siRNA treatments
  - Immunofluorescence staining
  - Intron RNA FISH combined with immunofluorescence
  - Live-cell imaging and drug treatment
  - Image processing and quantification
  - RT-qPCR
  - YAP and TEAD *in vitro* expression and purification
  - Differential Interference Contrast (DIC) microscopy of *in vitro* YAP and TEAD phase separation
  - Hexanediol treatment
  - Single-particle tracking (SPT) and analysis
- QUANTIFICATION AND STATISTICAL ANALYSIS

SUPPLEMENTAL INFORMATION

Supplemental information can be found online at https://doi.org/10.1016/j.isci.2024.109927.

ACKNOWLEDGMENTS

We appreciate the constructive feedback from Drs. Anthony Leung, Ashani Weeraratna, Duojia Pan, Bin Wu, and members of the Cai lab. We thank Dr. Jiou Wang for providing the pRK5-Myc-Fus-R495X plasmid. This work is supported by the National Institute of General Medical Sciences of the National Institutes of Health under Award Numbers R35GM142837 (D.C.) and R35GM137926 (S.S.), by a National Cancer Institute training grant T32CA009110 (J.D.), and by Howard Hughes Medical Institute (J.L.-O. and Z.L.).

AUTHOR CONTRIBUTIONS

Conceptualization, D.C.; methodology, D.C.; software, N.B.G. and Z.L.; validation, S.H. and Y.J.L.; formal analysis, S.H., Y.J.L., N.B.G., E.F., J.L., D.C., and H.F.; investigation, S.H., Y.J.L., N.B.G., E.F., J.L., H.F., D.C., and J.D.; resources, D.C., J.L.-S., Z.L., and S.S.; writing, D.C.; visualization, S.H., Y.J.L., N.B.G., and D.C.; supervision, D.C., J.L.-S., Z.L., and S.S.; project administration, D.C.; funding acquisition, D.C., J.L.-S., Z.L., and S.S.

DECLARATION OF INTERESTS

The authors declare no competing interests.

Received: November 10, 2022
Revised: October 24, 2023
Accepted: May 3, 2024
Published: May 7, 2024

REFERENCES

1. Zhao, B., Ye, X., Yu, J., Li, L., Li, W., Li, S., Yu, J., Lin, J.D., Wang, C.Y., Chinnaiyan, A.M., et al. (2008). TEAD mediates YAP-dependent gene induction and growth control. Genes Dev. *22*, 1962–1971. https://doi.org/10.1101/gad.1664408.
2. Zheng, Y., and Pan, D. (2019). The Hippo Signaling Pathway in Development and Disease. Dev. Cell *50*, 264–282. https://doi.org/10.1016/j.devcel.2019.06.003.
3. Meng, Z., Moroishi, T., and Guan, K.L. (2016). Mechanisms of Hippo pathway regulation. Genes Dev. *30*, 1–17. https://doi.org/10.1101/gad.274027.115.
4. Dupont, S., Morsut, L., Aragona, M., Enzo, E., Giulitti, S., Cordenonsi, M., Zanconato, F., Le Digabel, J., Forcato, M., Bicciato, S., et al. (2011). Role of YAP/TAZ in mechanotransduction. Nature *474*, 179–183. https://doi.org/10.1038/nature10137.
5. Elosegui-Artola, A., Andreu, I., Beedle, A.E.M., Lezamiz, A., Uroz, M., Kosmalska, A.J., Oria, R., Kechagia, J.Z., Rico-Lastres, P., Le Roux, A.L., et al. (2017). Force Triggers YAP Nuclear Entry by Regulating Transport across Nuclear Pores. Cell *171*, 1397–1410.e14. https://doi.org/10.1016/j.cell.2017.10.008.
6. Halder, G., Dupont, S., and Piccolo, S. (2012). Transduction of mechanical and cytoskeletal cues by YAP and TAZ. Nat. Rev. Mol. Cell Biol. *13*, 591–600. https://doi.org/10.1038/nrm3416.
7. Hong, A.W., Meng, Z., Yuan, H.X., Plouffe, S.W., Moon, S., Kim, W., Jho, E.H., and Guan, K.L. (2017). Osmotic stress-induced phosphorylation by NLK at Ser128 activates YAP. EMBO Rep. *18*, 72–86. https://doi.org/10.15252/embr.201642681.
8. Galli, G.G., Carrara, M., Yuan, W.C., Valdes-Quezada, C., Gurung, B., Pepe-Mooney, B., Zhang, T., Geeven, G., Gray, N.S., de Laat, W., et al. (2015). YAP Drives Growth by Controlling Transcriptional Pause Release from Dynamic Enhancers. Mol. Cell *60*, 328–337. https://doi.org/10.1016/j.molcel.2015.09.001.
9. Zanconato, F., Battilana, G., Forcato, M., Filippi, L., Azzolin, L., Manfrin, A., Quaranta, E., Di Biagio, D., Sigismondo, G., Guzzardo, V., et al. (2018). Transcriptional addiction in cancer cells is mediated by YAP/TAZ through BRD4. Nat. Med. *24*, 1599–1610. https://doi.org/10.1038/s41591-018-0158-8.
10. Cai, D., Feliciano, D., Dong, P., Flores, E., Gruebele, M., Porat-Shliom, N., Sukenik, S., Liu, Z., and Lippincott-Schwartz, J. (2019). Phase separation of YAP reorganizes genome topology for long-term YAP target gene expression. Nat. Cell Biol. *21*, 1578–1589. https://doi.org/10.1038/s41556-019-0433-z.
11. Yu, M., Peng, Z., Qin, M., Liu, Y., Wang, J., Zhang, C., Lin, J., Dong, T., Wang, L., Li, S., et al. (2021). Interferon-gamma induces tumor resistance to anti-PD-1 immunotherapy by promoting YAP phase separation. Mol. Cell *81*, 1216–1230.e9. https://doi.org/10.1016/j.molcel.2021.01.010.
12. Franklin, J.M., and Guan, K.L. (2020). YAP/TAZ phase separation for transcription. Nat. Cell Biol. *22*, 357–358. https://doi.org/10.1038/s41556-020-0498-8.
13. Lu, Y., Wu, T., Gutman, O., Lu, H., Zhou, Q., Henis, Y.I., and Luo, K. (2020). Phase separation of TAZ compartmentalizes the transcription machinery to promote gene expression. Nat. Cell Biol. *22*, 453–464. https://doi.org/10.1038/s41556-020-0485-0.
14. Banani, S.F., Lee, H.O., Hyman, A.A., and Rosen, M.K. (2017). Biomolecular condensates: organizers of cellular biochemistry. Nat. Rev. Mol. Cell Biol. *18*, 285–298. https://doi.org/10.1038/nrm.2017.7.
15. Jain, A., and Vale, R.D. (2017). RNA phase transitions in repeat expansion disorders. Nature *546*, 243–247. https://doi.org/10.1038/nature22386.
16. Shin, Y., and Brangwynne, C.P. (2017). Liquid phase condensation in cell physiology and disease. Science *357*, eaaf4382. https://doi.org/10.1126/science.aaf4382.
17. Grimm, J.B., English, B.P., Chen, J., Slaughter, J.P., Zhang, Z., Revyakin, A., Patel, R., Macklin, J.J., Normanno, D., Singer, R.H., et al. (2015). A general method to improve fluorophores for live-cell and single-molecule microscopy. Nat. Methods *12*, 244–250. 243 p following 250. https://doi.org/10.1038/nmeth.3256.
18. Li, H., Huang, Z., Gao, M., Huang, N., Luo, Z., Shen, H., Wang, X., Wang, T., Hu, J., and Feng, W. (2016). Inhibition of YAP suppresses CML cell proliferation and enhances efficacy of imatinib *in vitro* and *in vivo*. J. Exp. Clin. Cancer Res. *35*, 134.
19. Chen, X., Gu, W., Wang, Q., Fu, X., Wang, Y., Xu, X., and Wen, Y. (2018). C-MYC and BCL-2 mediate YAP-regulated tumorigenesis in OSCC. Oncotarget *9*, 668–679.
20. Oka, T., Mazack, V., and Sudol, M. (2008). Mst2 and Lats kinases regulate apoptotic function of Yes kinase-associated protein (YAP). J. Biol. Chem. *283*, 27534–27546. https://doi.org/10.1074/jbc.M804380200.
21. Coue, M., Brenner, S.L., Spector, I., and Korn, E.D. (1987). Inhibition of actin polymerization by latrunculin A. FEBS Lett. *213*, 316–318. https://doi.org/10.1016/0014-5793(87)81513-2.
22. Morton, W.M., Ayscough, K.R., and McLaughlin, P.J. (2000). Latrunculin alters the actin-monomer subunit interface to prevent polymerization. Nat. Cell Biol. *2*, 376–378. https://doi.org/10.1038/35014075.
23. Vasquez, R.J., Howell, B., Yvon, A.M., Wadsworth, P., and Cassimeris, L. (1997). Nanomolar concentrations of nocodazole alter microtubule dynamic instability *in vivo* and *in vitro*. Mol. Biol. Cell *8*, 973–985.
24. Kato, M., and McKnight, S.L. (2018). A Solid-State Conceptualization of Information Transfer from Gene to Message to Protein. Annu. Rev. Biochem. *87*, 351–390. https://doi.org/10.1146/annurev-biochem-061516-044700.
25. Ribbeck, K., and Görlich, D. (2002). The permeability barrier of nuclear pore complexes appears to operate via hydrophobic exclusion. EMBO J. *21*, 2664–2671. https://doi.org/10.1093/emboj/21.11.2664.
26. Cho, W.K., Spille, J.H., Hecht, M., Lee, C., Li, C., Grube, V., and Cisse, I.I. (2018). Mediator and RNA polymerase II clusters associate in transcription-dependent condensates. Science *361*, 412–415. https://doi.org/10.1126/science.aar4199.
27. Tulpule, A., Guan, J., Neel, D.S., Allegakoen, H.R., Lin, Y.P., Brown, D., Chou, Y.T., Heslin, A., Chatterjee, N., Perati, S., et al. (2021). Kinase-mediated RAS signaling via membraneless cytoplasmic protein granules. Cell *184*, 2649–2664.e18. https://doi.org/10.1016/j.cell.2021.03.031.
28. Shi, M., You, K., Chen, T., Hou, C., Liang, Z., Liu, M., Wang, J., Wei, T., Qin, J., Chen, Y., et al. (2021). Quantifying the phase separation property of chromatin-associated proteins under physiological conditions using an anti-1,6-hexanediol index. Genome Biol. *22*, 229. https://doi.org/10.1186/s13059-021-02456-2.
29. Liu, X., Jiang, S., Ma, L., Qu, J., Zhao, L., Zhu, X., and Ding, J. (2021). Time-dependent effect of 1,6-hexanediol on biomolecular condensates and 3D chromatin organization. Genome Biol. *22*, 230. https://doi.org/10.1186/s13059-021-02455-3.
30. Strano, S., Munarriz, E., Rossi, M., Castagnoli, L., Shaul, Y., Sacchi, A., Oren, M., Sudol, M., Cesareni, G., and Blandino, G. (2001). Physical interaction with Yes-associated protein enhances p73 transcriptional activity. J. Biol. Chem. *276*, 15164–15173. https://doi.org/10.1074/jbc.M010484200.
31. Vassilev, A., Kaneko, K.J., Shu, H., Zhao, Y., and DePamphilis, M.L. (2001). TEAD/TEF transcription factors utilize the activation domain of YAP65, a Src/Yes-associated protein localized in the cytoplasm. Genes Dev. *15*, 1229–1241. https://doi.org/10.1101/gad.888601.
32. Yagi, R., Chen, L.-F., Shigesada, K., Murakami, Y., and Ito, Y. (1999). A WW domain-containing yes-associated protein (YAP) is a novel transcriptional co-activator. EMBO J. *18*, 2551–2562.
33. Liu-Chittenden, Y., Huang, B., Shim, J.S., Chen, Q., Lee, S.J., Anders, R.A., Liu, J.O., and Pan, D. (2012). Genetic and pharmacological disruption of the TEAD-YAP complex suppresses the oncogenic activity of YAP. Genes Dev. *26*, 1300–1305. https://doi.org/10.1101/gad.192856.112.

34. Feng, J., Gou, J., Jia, J., Yi, T., Cui, T., and Li, Z. (2016). Verteporfin, a suppressor of YAP-TEAD complex, presents promising antitumor properties on ovarian cancer. OncoTargets Ther. *9*, 5371–5381. https://doi.org/10.2147/OTT.S109979.
35. Kandoussi, I., Lakhlili, W., Taoufik, J., and Ibrahimi, A. (2017). Docking analysis of verteporfin with YAP WW domain. Bioinformation *13*, 237–240. https://doi.org/10.6026/97320630013237.
36. Kaneda, A., Seike, T., Danjo, T., Nakajima, T., Otsubo, N., Yamaguchi, D., Tsuji, Y., Hamaguchi, K., Yasunaga, M., Nishiya, Y., et al. (2020). The novel potent TEAD inhibitor, K-975, inhibits YAP1/TAZ-TEAD protein-protein interactions and exerts an anti-tumor effect on malignant pleural mesothelioma. Am. J. Cancer Res. *10*, 4399–4415.
37. Zhang, Z., Lin, Z., Zhou, Z., Shen, H.C., Yan, S.F., Mayweg, A.V., Xu, Z., Qin, N., Wong, J.C., Zhang, Z., et al. (2014). Structure-Based Design and Synthesis of Potent Cyclic Peptides Inhibiting the YAP-TEAD Protein-Protein Interaction. ACS Med. Chem. Lett. *5*, 993–998. https://doi.org/10.1021/ml500160m.
38. Zhang, J., Pan, Y., Liao, D., Tang, J., and Yao, D. (2018). Peptide 17, an inhibitor of YAP/TEAD4 pathway, mitigates lung cancer malignancy. Trop. J. Pharm. Res. *17*, 1255–1262. https://doi.org/10.4314/tjpr.v17i7.5.
39. Wei, X., Jia, Y., Lou, H., Ma, J., Huang, Q., Meng, Y., Sun, C., Yang, Z., Li, X., Xu, S., et al. (2019). Targeting YAP suppresses ovarian cancer progression through regulation of the PI3K/Akt/mTOR pathway. Oncol. Rep. *42*, 2768–2776. https://doi.org/10.3892/or.2019.7370.
40. Song, S., Xie, M., Scott, A.W., Jin, J., Ma, L., Dong, X., Skinner, H.D., Johnson, R.L., Ding, S., and Ajani, J.A. (2018). A Novel YAP1 Inhibitor Targets CSC-Enriched Radiation-Resistant Cells and Exerts Strong Antitumor Activity in Esophageal Adenocarcinoma. Mol. Cancer Ther. *17*, 443–454. https://doi.org/10.1158/1535-7163.MCT-17-0560.
41. Hnisz, D., Abraham, B.J., Lee, T.I., Lau, A., Saint-André, V., Sigova, A.A., Hoke, H.A., and Young, R.A. (2013). Super-Enhancers in the Control of Cell Identity and Disease. Cell *155*, 934–947. https://doi.org/10.1016/j.cell.2013.09.053.
42. Hnisz, D., Shrinivas, K., Young, R.A., Chakraborty, A.K., and Sharp, P.A. (2017). A Phase Separation Model for Transcriptional Control. Cell *169*, 13–23. https://doi.org/10.1016/j.cell.2017.02.007.
43. Yang, Z., Yik, J.H.N., Chen, R., He, N., Jang, M.K., Ozato, K., and Zhou, Q. (2005). Recruitment of P-TEFb for stimulation of transcriptional elongation by the bromodomain protein Brd4. Mol. Cell *19*, 535–545.
44. Rahman, S., Sowa, M.E., Ottinger, M., Smith, J.A., Shi, Y., Harper, J.W., and Howley, P.M. (2011). The Brd4 Extraterminal Domain Confers Transcription Activation Independent of pTEFb by Recruiting Multiple Proteins, Including NSD3. Mol. Cell Biol. *31*, 2641–2652. https://doi.org/10.1128/Mcb.01341-10.
45. Plouffe, S.W., Lin, K.C., Moore, J.L., Tan, F.E., Ma, S., Ye, Z., Qiu, Y., Ren, B., and Guan, K.L. (2018). The Hippo pathway effector proteins YAP and TAZ have both distinct and overlapping functions in the cell. J. Biol. Chem. *293*, 11230–11240. https://doi.org/10.1074/jbc.RA118.002715.
46. Reggiani, F., Gobbi, G., Ciarrocchi, A., and Sancisi, V. (2021). YAP and TAZ Are Not Identical Twins. Trends Biochem. Sci. *46*, 154–168. https://doi.org/10.1016/j.tibs.2020.08.012.
47. Filippakopoulos, P., Qi, J., Picaud, S., Shen, Y., Smith, W.B., Fedorov, O., Morse, E.M., Keates, T., Hickman, T.T., Felletar, I., et al. (2010). Selective inhibition of BET bromodomains. Nature *468*, 1067–1073. https://doi.org/10.1038/nature09504.
48. Wagh, K., Garcia, D.A., and Upadhyaya, A. (2021). Phase separation in transcription factor dynamics and chromatin organization. Curr. Opin. Struct. Biol. *71*, 148–155. https://doi.org/10.1016/j.sbi.2021.06.009.
49. Liu, Z., Lavis, L.D., and Betzig, E. (2015). Imaging Live-Cell Dynamics and Structure at the Single-Molecule Level. Mol. Cell *58*, 644–659. https://doi.org/10.1016/j.molcel.2015.02.033.
50. Mehta, S., and Zhang, J. (2022). Liquid-liquid phase separation drives cellular function and dysfunction in cancer. Nat. Rev. Cancer *22*, 239–252. https://doi.org/10.1038/s41568-022-00444-7.
51. Irgen-Gioro, S., Yoshida, S., Walling, V., and Chong, S. (2022). Fixation Can Change the Appearance of Phase Separation in Living Cells. Preprint at bioRxiv. https://doi.org/10.1101/2022.05.06.490956.
52. Demmerle, J. (2019). Integrating Chromatin and Development: LDB1 Regulates Genome Architecture and Gene Expression in Motor Neuron Differentiation (University of Oxford).
53. Chen, K.H., Boettiger, A.N., Moffitt, J.R., Wang, S., and Zhuang, X. (2015). RNA imaging. Spatially resolved, highly multiplexed RNA profiling in single cells. Science *348*, aaa6090. https://doi.org/10.1126/science.aaa6090.
54. Fetiva, M.C., Liss, F., Gertzmann, D., Thomas, J., Gantert, B., Vogl, M., Sira, N., Weinstock, G., Kneitz, S., Ade, C.P., and Gaubatz, S. (2023). Oncogenic YAP mediates changes in chromatin accessibility and activity that drive cell cycle gene expression and cell migration. Nucleic Acids Res. *51*, 4266–4283. https://doi.org/10.1093/nar/gkad107.
55. Lian, I., Kim, J., Okazawa, H., Zhao, J., Zhao, B., Yu, J., Chinnaiyan, A., Israel, M.A., Goldstein, L.S.B., Abujarour, R., et al. (2010). The role of YAP transcription coactivator in regulating stem cell self-renewal and differentiation. Gene Dev. *24*, 1106–1118. https://doi.org/10.1101/gad.1903310.
56. Teves, S.S., An, L., Hansen, A.S., Xie, L., Darzacq, X., and Tjian, R. (2016). A dynamic mode of mitotic bookmarking by transcription factors. Elife *5*, e22280. https://doi.org/10.7554/eLife.22280.
57. Liu, Z., Legant, W.R., Chen, B.-C., Li, L., Grimm, J.B., Lavis, L.D., Betzig, E., and Tjian, R. (2014). 3D imaging of Sox2 enhancer clusters in embryonic stem cells. Elife *3*, e04236.
58. Garcia, D.A., Johnson, T.A., Presman, D.M., Fettweis, G., Wagh, K., Rinaldi, L., Stavreva, D.A., Paakinaho, V., Jensen, R.A.M., Mandrup, S., et al. (2021). An intrinsically disordered region-mediated confinement state contributes to the dynamics and function of transcription factors. Mol. Cell *81*, 1484–1498.e6.
59. McSwiggen, D.T., Hansen, A.S., Teves, S.S., Marie-Nelly, H., Hao, Y., Heckert, A.B., Umemoto, K.K., Dugast-Darzacq, C., Tjian, R., and Darzacq, X. (2019). Evidence for DNA-mediated nuclear compartmentalization distinct from phase separation. Elife *8*, e47098. https://doi.org/10.7554/eLife.47098.
60. Chong, S., Graham, T.G.W., Dugast-Darzacq, C., Dailey, G.M., Darzacq, X., and Tjian, R. (2022). Tuning levels of low-complexity domain interactions to modulate endogenous oncogenic transcription. Mol. Cell *82*, 2084–2097.e5. https://doi.org/10.1016/j.molcel.2022.04.007.
61. Darling, A.L., and Shorter, J. (2021). Combating deleterious phase transitions in neurodegenerative disease. Biochim. Biophys. Acta Mol. Cell Res. *1868*, 118984. https://doi.org/10.1016/j.bbamcr.2021.118984.
62. Portz, B., Lee, B.L., and Shorter, J. (2021). FUS and TDP-43 Phases in Health and Disease. Trends Biochem. Sci. *46*, 550–563. https://doi.org/10.1016/j.tibs.2020.12.005.
63. Cai, D., Liu, Z., and Lippincott-Schwartz, J. (2021). Biomolecular Condensates and Their Links to Cancer Progression. Trends Biochem. Sci. *46*, 535–549. https://doi.org/10.1016/j.tibs.2021.01.002.
64. Jiang, S., Fagman, J.B., Chen, C., Alberti, S., and Liu, B. (2020). Protein phase separation and its role in tumorigenesis. Elife *9*, e60264. https://doi.org/10.7554/eLife.60264.
65. Lu, J., Qian, J., Xu, Z., Yin, S., Zhou, L., Zheng, S., and Zhang, W. (2021). Emerging Roles of Liquid-Liquid Phase Separation in Cancer: From Protein Aggregation to Immune-Associated Signaling. Front. Cell Dev. Biol. *9*, 631486. https://doi.org/10.3389/fcell.2021.631486.
66. Hutten, S., Usluer, S., Bourgeois, B., Simonetti, F., Odeh, H.M., Fare, C.M., Czuppa, M., Hruska-Plochan, M., Hofweber, M., Polymenidou, M., et al. (2020). Nuclear import receptors directly bind to arginine-rich dipeptide repeat proteins and suppress their pathological interactions. Cell Rep. *33*, 108538.
67. Mitrea, D.M., Mittasch, M., Gomes, B.F., Klein, I.A., and Murcko, M.A. (2022). Modulating biomolecular condensates: a novel approach to drug discovery. Nat. Rev. Drug Discov. *21*, 841–862. https://doi.org/10.1038/s41573-022-00505-4.
68. Zhang, T., Wu, Y.C., Mullane, P., Ji, Y.J., Liu, H., He, L., Arora, A., Hwang, H.Y., Alessi, A.F., Niaki, A.G., et al. (2018). FUS Regulates Activity of MicroRNA-Mediated Gene Silencing. Mol. Cell *69*, 787–801.e8. https://doi.org/10.1016/j.molcel.2018.02.001.
69. Liu, H., Dong, P., Ioannou, M.S., Li, L., Shea, J., Pasolli, H.A., Grimm, J.B., Rivlin, P.K., Lavis, L.D., Koyama, M., and Liu, Z. (2018). Visualizing long-term single-molecule dynamics *in vivo* by stochastic protein labeling. Proc. Natl. Acad. Sci. USA *115*, 343–348. https://doi.org/10.1073/pnas.1713895115.
70. Teves, S.S., An, L., Hansen, A.S., Xie, L., Darzacq, X., and Tjian, R. (2016). A dynamic mode of mitotic bookmarking by transcription factors. Elife *5*, e22280.
71. Normanno, D., Boudarène, L., Dugast-Darzacq, C., Chen, J., Richter, C., Proux, F., Bénichou, O., Voituriez, R., Darzacq, X., and Dahan, M. (2015). Probing the target search of DNA-binding proteins in mammalian cells using TetR as model searcher. Nat. Commun. *6*, 7357. https://doi.org/10.1038/ncomms8357.

72. Li, L., Liu, H., Dong, P., Li, D., Legant, W.R., Grimm, J.B., Lavis, L.D., Betzig, E., Tjian, R., and Liu, Z. (2016). Real-time imaging of Huntingtin aggregates diverting target search and gene transcription. Elife *5*, e17056. https://doi.org/10.7554/eLife.17056.

73. Tarantino, N., Tinevez, J.Y., Crowell, E.F., Boisson, B., Henriques, R., Mhlanga, M., Agou, F., Israël, A., and Laplantine, E. (2014). TNF and IL-1 exhibit distinct ubiquitin requirements for inducing NEMO-IKK supramolecular structures. J. Cell Biol. *204*, 231–245. https://doi.org/10.1083/jcb.201307172.

74. Sergé, A., Bertaux, N., Rigneault, H., and Marguet, D. (2008). Dynamic multiple-target tracing to probe spatiotemporal cartography of cell membranes. Nat. Methods *5*, 687–694.

75. Gomez-Garcia, P.A., Portillo-Ledesma, S., Neguembor, M.V., Pesaresi, M., Oweis, W., Rohrlich, T., Wieser, S., Meshorer, E., Schlick, T., Cosma, M.P., and Lakadamyali, M. (2021). Mesoscale Modeling and Single-Nucleosome Tracking Reveal Remodeling of Clutch Folding and Dynamics in Stem Cell Differentiation. Cell Rep. *34*, 108614. https://doi.org/10.1016/j.celrep.2020.108614.

STAR★METHODS

KEY RESOURCES TABLE

REAGENT or RESOURCE	SOURCE	IDENTIFIER
Antibodies		
Anti-YAP antibody	Cell Signaling Technology	Cat#14074S; RRID: AB_2650491
Anti-TEAD1 antibody	BD Biosciences	Cat#610922; RRID: AB_398237
Anti-BRD4 antibody	Sigma-Aldrich	Cat#HPA015055; RRID: AB_1845435
Goat anti-Rabbit IgG (H+L) Cross-Adsorbed Secondary Antibody, Alexa Fluor 568	Thermo Fisher Scientific	Cat#A11011; RRID: AB_143157
Goat anti-Rabbit IgG (H+L) Cross-Adsorbed Secondary Antibody, Alexa Fluor 488	Thermo Fisher Scientific	Cat#A11034; RRID: AB_2576217
Goat anti-Mouse IgG (H+L) Cross-Adsorbed Secondary Antibody, Alexa Fluor 568	Thermo Fisher Scientific	Cat#A11031; RRID: AB_144696
Goat anti-Mouse IgG (H+L) Cross-Adsorbed Secondary Antibody, Alexa Fluor 488	Thermo Fisher Scientific	Cat#A11001; RRID: AB_2534069
Bacterial and virus strains		
DH5α Competent Cells	Thermo Fisher Scientific	Cat#EC0112
BL-21(DE3) Competent Cells	Agilent	Cat#200131
Chemicals, peptides, and recombinant proteins		
Verteporfin	Sigma	Cat#SML0534
K-975	MedChemExpress	Cat#HY-138565
Peptide 17	SelleckChem	Cat#S8164
CA3	Sigma	Cat#SML2647
Fetal Bovine Serum	Gibco	Cat#26140079
Dulbecco's Modified Eagle Medium	Corning	Cat#15-013-CV
GlutaMAX-I	Gibco	Cat#35050061
Penicillin/streptomycin	Thermo Fisher Scientific	Cat#15140122
Fibronectin	Millipore	Cat#FC010
Formaldehyde	Cell Signaling Technology	Cat#12606S
Triton X-100	Sigma-Aldrich	Cat#T8787
Bovine serum albumin	Millipore Sigma	Cat#A7906
FluoroBrite DMEM Complete Medium	Gibco	Cat#A1896701
cOmplete Mini Protease Inhibitor Cocktail tablet	Roche	Cat#11836153001
1,6-Hexanediol	Sigma-Aldrich	Cat#240117
2,5-Hexanediol	Sigma-Aldrich	Cat#H11904
AmyTracker680	Ebba Biotech	N/A
Hoechst 33342	Thermo Fisher Scientific	Cat#62249
Janelia Fluor (JF) 549 Halo Dye	Luke Lavis[17]	N/A
Critical commercial assays		
Lipofectamine 3000 Transfection Reagent	Thermo Fisher Scientific	Cat#L3000015
Lipofectamine RNAiMAX Transfection Reagent	Thermo Fisher Scientific	Cat#13778075
Direct-zol RNA MiniPrep Kit	Zymo Research	Cat#R2052
High Capacity RNA-to-cDNA reverse transcription kit	Thermo Fisher Scientific	Cat#4387406
PowerUp SYBR Green Master Mix	Thermo Fisher Scientific	Cat#A25742
Stellaris RNA FISH Hybridization Buffer	Biosearch Technologies	Cat#SMF-HB1-10

(*Continued on next page*)

Continued

REAGENT or RESOURCE	SOURCE	IDENTIFIER
Stellaris RNA FISH Wash Buffer A	Biosearch Technologies	Cat#SMF-WA1-60
Stellaris RNA FISH Wash Buffer B	Biosearch Technologies	Cat#SMF-WB1-20
Deposited data		
All tracks and masks associated with single-particle tracking	Zenodo	https://doi.org/10.5281/zenodo.10980638
Experimental models: Cell lines		
U-2 OS	ATCC	Cat#HTB-96
YAP–HaloTag CRISPR knock-in U-2 OS cells	Danfeng Cai[10]	N/A
Oligonucleotides		
Lats1 siRNA	Thermo Fisher Scientific	Silencer Select s17393
Lats2 siRNA	Thermo Fisher Scientific	Silencer Select s25503
TEAD1 siRNA	Thermo Fisher Scientific	Silencer Select s13962
Scrambled negative control siRNA	Thermo Fisher Scientific	Cat#AM4611
Human *MYC*_intron with Quasar 570 dye	Biosearch Technologies	Cat#ISMF-2066-5
Human *ACTB*_intron with Quasar 570 dye	Biosearch Technologies	Cat#ISMF-2002-5
Recombinant DNA		
pEGFP-C3-Lats1 plasmid	Addgene[20]	Addgene plasmid #19053
pEGFP-C3-Mst2 plasmid	Addgene[20]	Addgene plasmid #19056
pRK5-Myc-Fus-R495X plasmid	Jiou Wang[68]	N/A
EGFP-TAZ plasmid	Danfeng Cai[10]	N/A
PB-EF1-HaloTag-H2B	Zhe Liu[69]	N/A
Software and algorithms		
ImageJ	National Institutes of Health	https://imagej.nih.gov/ij/
FIJI (Fiji Is Just ImageJ)	ImageJ/Fiji	https://fiji.sc/
MATLAB	MathWorks	https://www.mathworks.com/
Coloc 2 plugin for ImageJ	ImageJ/Fiji	https://imagej.net/plugins/coloc-2
BIOP JACoP plugin for Fiji	ImageJ/Fiji	https://imagej.net/plugins/jacop
SLIMfast.m (MATLAB code)	Robert Tjian[70]; Maxime Dahan[71]	N/A
RegionalDiffusionMap.m (MATLAB code)	Zhe Liu[72]	N/A
msdanalyzer (MATLAB code)	Tarantino et al.[73]	N/A

RESOURCE AVAILABILITY

Lead contact

Further information and requests for resources and reagents should be directed to and will be fulfilled by the lead contact, Danfeng Cai (danfeng.cai@jhu.edu).

Materials availability

This study did not generate new unique reagents.

Data and code availability

- All data associated with SPT is deposited to Zenodo and publicly available (Zenodo: https://doi.org/10.5281/zenodo.10980638). All other data reported in this paper will be shared by the lead contact upon request.
- All original code is available in this paper's supplemental information: Data S2 and S3.
- Any additional information required to reanalyze the data reported in this paper is available from the lead contact upon request.

EXPERIMENTAL MODEL AND STUDY PARTICIPANT DETAILS

Cell lines

U-2 OS (ATCC, HTB-96) and YAP–HaloTag CRISPR knock-in U-2 OS cells[10] were cultured at 37°C and 5% CO_2 in DMEM supplemented with 10% fetal bovine serum (FBS; Gibco, 26140079), 100 U/ml (1%) penicillin/streptomycin (Gibco, 15140122) and 2 mM (1%) GlutaMAX-I (Gibco, 35050061). Sexes of cells are female. Cells are authenticated every three months at Genetic Resources Core Facility at Johns Hopkins University, using STR profiling following ANSI/ATCC ASN-0002-2011, Authentication of Human Cell Lines: Standardization of STR Profiling guidelines. Cell lines are also tested for mycoplasma contamination every three months using a MycoStrip™ – Mycoplasma Detection Kit.

METHOD DETAILS

Transfection and siRNA treatments

For overexpression experiments, YAP–HaloTag CRISPR knock-in U-2 OS cells were transfected with pEGFP-C3-Lats1 (Addgene plasmid # 19053) or pEGFP C3-Mst2 (Addgene plasmid # 19056), both gifts from Marius Sudol, pRK5-Myc-Fus-R495X,[68] gift from Jiou Wang, or EGFP-TAZ (made in the Cai lab) using Lipofectamine 3000 Transfection Reagent (cat. no. L3000015), for 16 h. For RNAi experiments, a mixture of Lats1 siRNA (Thermo Fisher, Silencer Select s17393) and Lats2 siRNA (Thermo Fisher, Silencer Select s25503) was used at a final concentration of 10 nM, or the scrambled negative control siRNA was used at a final concentration of 20 nM (Thermo Fisher, AM4611), and were transfected into cells using the Lipofectamine RNAiMAX transfection reagent (Thermo Fisher, cat. no. 13778075) for 48 h. For siTEAD1 experiments, the TEAD1 siRNA (Thermo Fisher, Silencer Select s13962) or scrambled negative control siRNA was used at a final concentration of 10 nM (Thermo Fisher, AM4611), and were transfected into cells using the Lipofectamine RNAiMAX transfection reagent (Thermo Fisher, cat. no. 13778075) for 48 h, after which cells were replated for live cell imaging and RT-qPCR.

Immunofluorescence staining

After transfection, YAP–HaloTag CRISPR knock-in U-2 OS cells were plated on coverslips pre-coated with fibronectin (7.5 μg/mL; Millipore, FC010). Cells were grown for 20 hours and fixed with 4% formaldehyde (Cell Signaling Technology, 12606S), permeabilized with 0.1% Triton X-100, and blocked with 3% BSA in 1X PBS. The cells were then incubated overnight with primary antibodies in 1% BSA at 4°C, and then incubated with Alexa Fluor-conjugated secondary antibodies in 1% BSA for 1 h at RT. The following primary and secondary antibodies were used: anti-YAP (1:150; Cell Signaling, 14074S); anti-TEAD1 (BD Biosciences; 610922); anti-BRD4 (Sigma; HPA015055); Goat anti-Rabbit IgG (H+L) Cross-Adsorbed Secondary Antibody, Alexa Fluor 568 (1:1000; Thermo fisher, A11011). Protein amyloid aggregates were stained with AmyTracker680 (1:1000; Ebba Biotech) in PBS. Nuclei were labeled with 1:5000 Hoechst 33342 (Thermo Fisher, cat. no. 62249). For imaging and quantification, at least 20 fields of view per coverslip were randomly chosen by Hoechst nuclear staining, and imaged using a Zeiss LSM900 Airyscan microscope, followed by Airyscan processing (2D, default settings). The number of foci were counted with an in-house ImageJ script. For overexpression and RNAi experiments, the threshold was 1700 (a.u.), size 0.015, and 2400, size 0.015, respectively. At least three different coverslips from separate experiments were quantified per treatment type.

Intron RNA FISH combined with immunofluorescence

Human *MYC*_intron with Quasar 570 dye (Biosearch Technologies, ISMF-2066-5), human *ACTB*_intron with Quasar 570 dye (Biosearch Technologies, ISMF-2002-5), Stellaris RNA FISH Hybridization Buffer (Biosearch Technologies, SMF-HB1-10), Stellaris RNA FISH Wash Buffer A (Biosearch Technologies, SMF-WA1-60) and Wash Buffer B (Biosearch Technologies, SMF-WB1-20) are purchased from Biosearch Technologies. We followed the protocol for sequential IF + FISH in Adherent Cells listed on the Biosearch Technologies website listed under Stellaris RNA FISH protocols.

Live-cell imaging and drug treatment

The YAP–HaloTag CRISPR knock-in U-2 OS cells were plated into eight-well LabTek chambered coverglass dishes (life technologies, 155409PK) for drug treatment and imaging the following day. Before drug treatment, the cells were labeled with a mixture of Janelia Fluor (JF) 549 Halo dye and Hoechst 33342 (Thermo Fisher, 62249) for 30 min, to a final concentration of 0.1 μM and 2 μM, respectively. Then, the media was replaced with FluoroBrite DMEM Complete Medium (Gibco, A1896701) supplemented with 10% fetal bovine serum (FBS; Gibco, 26140079) and 2 mM GlutaMAX-I (Gibco, 35050061). All drugs were resuspended in dimethylsulfoxide (DMSO). Endogenous YAP condensates are naturally occurring and not induced with sorbitol, unless specifically noted. Images were taken before, 0.5 h and 1 h after drug treatments. DMSO was used as the negative control. The final concentrations of the drugs were: Verteporfin: 50 nM; K-975: 500 nM; Peptide 17: 500 nM; and CA-3: 500 nM. For imaging, at least 10 fields of view per coverslip were randomly chosen by Hoechst nuclear staining and imaged using a Zeiss LSM900 Airyscan microscope, followed by Airyscan processing (2D, default settings). For 2D imaging of YAP condensates, we choose the z-plane which shows the largest nuclear area visualized by the Hoechst dye.

Image processing and quantification

YAP condensates were counted with an in-house ImageJ script (Data S4), with a pixel intensity threshold of 400 and a size threshold of 0.015 μm^3. At least two different coverslips from separate experiments and 20 cells per replicate were quantified per treatment type. To

calculate colocalization between two channels, we used an ImageJ plugin Coloc 2 to derive Pearson correlation coefficient (PCC), which is the ratio between the covariance of two variables and the product of their standard deviations. PCC is commonly used to assess the similarity or correlation between the pixel intensities of corresponding pixels in two images. Unless otherwise noted, we only calculated the PCC of nuclear intensity signals, using the nuclear dye Hoechst as a mask. To calculate the enrichment of BRD4 signal at YAP condensates, we used a 1.48 μm x 1.48 μm region of interest (ROI) box to center around 10s of individual YAP condensates in 2D immunofluorescence images using ImageJ, and duplicated both YAP-HaloTag and BRD4 channels. The duplicated smaller images are then combined into stacks of either YAP-HaloTag or BRD4 channels, and the averaged images are derived using the Z-project-> Average function in ImageJ. For TEAD1/YAP colocalization, a square region measuring 3.01 μm by 3.01 μm was delineated around the focal points of YAP1. Additionally, a negative control square was randomly selected within the nucleoplasm where YAP1 staining appeared diffused. The colocalization analysis was conducted using the FIJI software with BIOP JACoP plugin. Statistical evaluation was performed using an unpaired T-test, specifically focusing on the Manders' overlap coefficient (Coloc 2 plugin of ImageJ) to assess the degree of colocalization between TEAD1 and YAP.

RT-qPCR

Total RNA was isolated from YAP–HaloTag CRISPR knock-in U-2 OS cells using the Direct-zol RNA MiniPrep kit (cat. no. R2052) and converted to complementary DNA using the Thermo Fisher High Capacity RNA-to-cDNA Reverse Transcription Kit (cat. no. 4387406). The RT-qPCR was carried out on a QuantStudio 3 Real-Time PCR Instrument using PowerUp SYBR Green Master Mix (Thermo Fisher, cat. no. A25742). The primers used were listed in Table S1. mRNA levels were normalized to those of *GAPDH*. For *GAPDH* levels in JQ-1 treatment experiments, we used the CT value of *GAPDH* to show it didn't change after JQ-1 treatment.

YAP and TEAD *in vitro* expression and purification

pET28b-YAP and pET28b-TEAD were expressed individually, using the same following protocol. BL-21(DE3) competent cells (Agilent) were transformed with the plasmids following supplier protocol and plated on LB agar plated with kanamycin selection overnight at 37°C. Transformed cells were expressed in 6 L of LB at pH 7.4 with kanamycin selection. Expression was induced at OD600 of 0.6 using 0.5 mM IPTG, and cells were left under shaking at 220 RPM and 16°C for 20h prior to collection. Collected cells were spun down at 4°C for 15 min and the supernatant was discarded. The pellet was resuspended with 20 mL lysis buffer (50 mM NaH2PO4, 0.5 M NaCl, pH 8) and 1 cOmplete Mini Protease Inhibitor Cocktail tablet (Roche) per 1 L of expression, and the resuspended cells were lysed via homogenization for 8 min (Emulsiflex homogenizer) or via sonication (QsonicaQ700, 0.5 inch tip). The resulting cell lysate was spun down for 50 min at 19,500 g, and the supernatant was collected. Ni-NTA nickel beads (QIAGEN) were equilibrated with lysis buffer (50 mM NaH2PO4, 0.5 M NaCl, pH 8), then loaded with the lysate and washed with 50 mL of wash buffer (50 mM NaH2PO4, 0.5 M NaCl, 20 mM Imidazole, pH 8) followed by 8 mL of Elution Buffer (50 mM NaH2PO4, 0.5 M NaCl, 250 mM Imidazole, pH 8) all done at 4°C. The eluent was collected, spun down to remove aggregates, and further purified with size exclusion chromatography (SEC) using a Superdex 200 16/60 column (GE) equilibrated using a 20 mM TRIS, 150 mM NaCl and pH 8 buffer (pH 7 for YAP). 5 mL of spun-down eluent was injected onto the column and ran at 0.5 mL/min at room temperature. Fractions were collected and the presence and purity of the protein was verified using SDS-PAGE (Data S1).

Differential Interference Contrast (DIC) microscopy of *in vitro* YAP and TEAD phase separation

All DIC images were in 20 mM TRIS, 150 mM NaCl and pH 8 buffer. YAP only images were taken at a 15 μM concentration. TEAD only images were taken at a 20 μM concentration. 20% wt/wt PEG 2000 in 20 mM TRIS, 150 mM NaCl and pH 8 buffer was mixed with TEAD for a final concentration of 15 μM. 15 μM of YAP and TEAD were mixed together to induce phase separation. WTYAP and TEAD were mixed with shown concentrations. All images were taken within 10 minutes after sample preparation. 8 well silicone gaskets (Grace Biolabs) were used as chambers and placed on a Fisherbrand glass microscopy slide. 21 μL of sample were placed in each well and sealed with a #1.5 coverslip. DIC images were taken on a Zeiss Observer 3 inverted microscope using a 40x 0.9 NA dry objective. Images were taken using a Hamamatsu Orca Flash v3.0 camera with an exposure time of 100 ms.

Hexanediol treatment

For treating live cell, we plated U-2 OS YAP-HaloTag cells in eight-well LabTek chambered coverglass dishes as described, stained them with Halo dye and Hoechst dye as described. Airyscan live-cell images of individual cells were taken pretreatment and 10 min after 1% 1,6-hexandiol treatment. For hexandiol treatment of *in vitro* YAP condensates, 8.5uM of purified EGFP-YAP protein was allowed to undergo phase separation with the addition of 10% PEG. 1,6-hexanediol or control 2,5-hexanediol was added to the YAP protein solution within the concentration range of 0%-15%. After 30 min, the degree of YAP phase separation was inferred by measuring the solution absorbance of 600 nm light.

Single-particle tracking (SPT) and analysis

SPT experiments for Halo-tagged YAP protein were conducted on a custom-built Nikon Eclipse TiE motorized inverted microscope equipped with a 100x Oil-immersion TIRF objective lens (Nikon, N.A. = 1.49), four laser lines (405/488/561/647 nm), an automatic TIRF illuminator, a PerfectFocus™ system, a tri-cam splitter, three EMCCDs (iXon Ultra 897, Andor) and Tokai Hit environmental control system (humidity, 37°C, 5% CO_2). The TIRF illuminator was adjusted to deliver a highly inclined and laminated optical sheet (HILO) to the cover glass, with the incident angle smaller than the critical angle. Thus, the laser beam was laminated to form a light-sheet above the cover glass. U-2 OS

YAP-HaloTag cells were sparsely labelled with 10 nM JF646 Halo dye at 37°C for 15 min, washed with fresh medium 3 times, and replaced with phenol red-free FluoBrite medium. Single molecules of YAP were imaged using a 647 nm laser at 100% laser power (3~5kw/cm^2 at focal plane). In U-2 OS HaloTag cells transfected with EGFP-TAZ, we used an additional 488 nm laser to excite the EGFP-TAZ channel using around 5% laser power. YAP-HaloTag single molecules and EGFP-TAZ were simultaneously captured using two EMCCD cameras with a 20 ms acquisition time for 10,000 frames and a total time of 200 s. For SPT of H2B proteins, we transfected the U-2 OS cells with a PB-EF1-HaloTag-H2B construct as previously described.[69] One day after transfection, we labelled H2B with 10 nM JF646 Halo dye for 15 min, washed, and performed SPT on the same microscope with a similar set up.

For 2D single-molecule localization and tracking of YAP and H2B, the spot localization (x,y) was obtained through 2D Gaussian fitting using a MATLAB code called SLIMfast.m,[70,71] based on the tracking algorithm Multiple Target Tracking (MTT).[74] The following parameters were used: pixel size: 0.16; emission: 664 nm; N.A.: 1.49; Lag time: 20 ms. After localizing all the molecules, we performed tracking with the same SLIMfast.m module (max diffusion coefficient: 1; max off-time: 3). Then, for simple derivation of diffusion coefficients inside and outside of condensates, we used a custom MATLAB code called "RegionalDiffusionMap.m".[72]

Mock compartment generation: Mock compartments were generated in a manner similar to that previously described.[60] Individual EGFP-TAZ condensates were independently allocated a random initial position in the nucleus, after which point they moved in the same manner as they did in the biological condensate relative to their new initial position. If after random allocation a compartment overlapped with another or exited the nucleus at any frame the mask was regenerated until a valid set of mock compartments was formed. In lieu of a nuclear marker, the nucleus was first segmented manually in the initial and final frames using ImageJ. A line was then drawn between each pixel on the perimeter of the initial nuclear mask to the closest pixel in the perimeter of the final mask. The nucleus was estimated as the convex hull of the resulting shape in the two spatial dimensions and time. Nuclear approximations that did not contain the original condensates at all frames were retraced.

Diffusion coefficient calculation: MATLAB code msdanalyzer[73] along with custom MATLAB codes were used. YAP tracks were classified as either inside or outside a condensate (or mock condensate). Only the first four frames of each trajectory were used to calculate diffusion coefficients to avoid bias resulting from the boundary, as done previously.[75] All trajectories shorter than four frames were rejected, along with trajectories whose initial four frames spanned more than 100ms (again to ensure short time frames consistent with an assumption of pure Brownian motion). The four data points (including origin) were then fit on a linear time-MSD plot assuming pure two-dimensional diffusive behavior:

$$\langle r^2 \rangle = 4Dt$$

Diffusion coefficients were only obtained for data well-fit by the linear approximation, requiring $R^2 \geq 0.8$ (including the origin).

In total 27 cells were imaged for YAP tracks and 18 were imaged for H2B tracks. After rejecting trajectories shorter than 4 frames, and ones whose initial four frames are more than 100ms apart, and ones whose initial four frames fit a linear proportionality poorly ($R^2 < 0.8$), we had the following number of trajectories remaining (each yielding a single diffusion coefficient): outside original condensates: 5416 trajectories; inside original condensates: 503 trajectories; inside mock condensates: 181 trajectories; and H2B: 5731 trajectories.

All codes used for data analysis and visualization are included in Data S2 and S3.

QUANTIFICATION AND STATISTICAL ANALYSIS

We used the statistical analysis tools in the GraphPad Prism software for quantification and statistical analysis. All of the statistical details of experiments can be found in the figure and figure legends, including the statistical tests used, exact value of n, what n represents, definition of center, and dispersion and precision measures.